

# Prediction of welding residual stresses using machine learning: Comparison between neural networks and neuro-fuzzy systems

Mathew, J, Griffin, J, Alamaniotis, M, Kanarachos, S & Fitzpatrick, M

Author post-print (accepted) deposited by Coventry University's Repository

Original citation & hyperlink:

Mathew, J, Griffin, J, Alamaniotis, M, Kanarachos, S & Fitzpatrick, M 2018, 'Prediction of welding residual stresses using machine learning: Comparison between neural networks and neuro-fuzzy systems' *Applied Soft Computing*, vol 70, pp. 131-146.

<https://dx.doi.org/10.1016/j.asoc.2018.05.017>

DOI [10.1016/j.asoc.2018.05.017](https://dx.doi.org/10.1016/j.asoc.2018.05.017)

ISSN 1568-4946

Publisher: Elsevier

**NOTICE: this is the author's version of a work that was accepted for publication in *Applied Soft Computing*. Changes resulting from the publishing process, such as peer review, editing, corrections, structural formatting, and other quality control mechanisms may not be reflected in this document. Changes may have been made to this work since it was submitted for publication. A definitive version was subsequently published in *Applied Soft Computing*, VOL 70, (2018)**

DOI: [10.1016/j.asoc.2018.05.017](https://dx.doi.org/10.1016/j.asoc.2018.05.017)

© 2017, Elsevier. Licensed under the Creative Commons Attribution-NonCommercial-NoDerivatives 4.0 International  
<http://creativecommons.org/licenses/by-nc-nd/4.0/>

Copyright © and Moral Rights are retained by the author(s) and/ or other copyright owners. A copy can be downloaded for personal non-commercial research or study, without prior permission or charge. This item cannot be reproduced or quoted extensively from without first obtaining permission in writing from the copyright holder(s). The content must not be changed in any way or sold commercially in any format or medium without the formal permission of the copyright holders.

This document is the author's post-print version, incorporating any revisions agreed during the peer-review process. Some differences between the published version and this version may remain and you are advised to consult the published version if you wish to cite from it.

# **Prediction of welding residual stresses using machine learning: Comparison between neural networks and neuro-fuzzy systems**

J. Mathew<sup>a\*</sup>, J. Griffin<sup>a</sup>, M. Alamaniotis<sup>b</sup>, S. Kanarachos<sup>a</sup>, M.E. Fitzpatrick<sup>a</sup>

<sup>a</sup>*Faculty of Engineering, Environment and Computing, Coventry University, Priory Street, Coventry CV1 5FB, United Kingdom*

<sup>b</sup>*School of Nuclear Engineering, Purdue University, West Lafayette, IN 47907, USA*

*Corresponding author email: [Jino.Mathew@coventry.ac.uk](mailto:Jino.Mathew@coventry.ac.uk)*

## **Abstract**

Safe and reliable operation of power plants invariably relies on the structural integrity assessments of pressure vessels and piping systems. Welded joints are a potential source of failure, because of the combination of the variation in mechanical properties and the residual stresses associated with the thermomechanical cycles experienced by the material during welding. This paper presents comparative studies between methods based on artificial neural networks (ANN) and fuzzy neural networks (FNN) for predicting residual stresses induced by welding. The performance of neural network and neuro-fuzzy systems are compared based on statistical indicators, scatter plots and several case studies. Results show that the neuro-fuzzy systems optimised using a hybrid technique can perform slightly better than a neural network trained using Levenberg-Marquardt algorithm, primarily because of the inability of the ANN approach to provide conservative estimates of residual stress profiles. Specifically, the prediction accuracy of the neuro-fuzzy systems trained using the hybrid technique is better for the axial residual stress component, with root mean square error ( $RMSE$ ), absolute fraction of variance ( $R^2$ ) and mean absolute percentage error ( $MAPE$ ) error of 0.1264, 0.9102 and 22.9442 respectively using the test data. Furthermore, this study demonstrates the potential benefits of implementing

neuro-fuzzy systems in predicting residual stresses for use in structural integrity

assessment of power plant components.

**Keywords:** Artificial neural networks, Adaptive neuro-fuzzy inference system (ANFIS), welding, residual stress

## 1 Introduction

Residual stresses can be generated in pressure vessel and piping systems as a

consequence of manufacturing process such as welding. Structural integrity

assessment of welded components must take account of residual stresses remaining in

the welded joint as well as the applied service loading conditions. Tensile residual

stresses in engineering structures can be detrimental as they can initiate cracks or

accelerate growth of pre-existing cracks during service. Engineering fracture

assessment procedures such as R6 [1] and API-579 [2] provide guidelines on the

treatment of residual stresses. In undertaking safety assessments of welds, estimations

are generally made of the residual stresses, and in order to provide both simplicity and

conservatism, yield levels of residual stresses may be assumed. These estimated

residual stress distributions in welded components can then lead to conservatism in

the predicted plant life and may unfavourably affect the life extension scenarios of

operating power plants.

The use of mechanistic approaches such as finite element modelling [3] often rely on the modeller's choice of assumptions and there is significant uncertainty

owing to the inherent complexity of the welding process. Moreover, finite element

simulation requires extensive computational requirements and tedious non-linear

analysis of the welding process, limiting its application to safety-critical components

that require a high standard of validation [4]. The finite element approach for

predicting weld residual stresses requires comprehensive data such as the physical and

thermo-physical properties from room temperature up to the melting point, parameters for all beads deposited during welding, and tensile and cyclic stress-strain data of weld and parent material [5]. A series of round-robin activities have been undertaken recently for the improvement of the numerical techniques in order to reliably characterise the distribution of residual stresses in structural welds [6, 7].

With the development of residual stress measurement techniques, both non-destructive and destructive, extensive experimental data are readily becoming available on residual stresses in welds. Neutron diffraction [8] is a popular non-destructive technique that can be used to determine the residual stress distribution in thick-section welds because of its high depth of penetration and good spatial resolution that is capable of resolving high strain gradients. Neutron diffraction is based on the principle of Bragg's law to measure the changes in lattice spacing of the material's crystallographic planes. By contrast, destructive methods such as the contour method [9] and deep hole drilling [10] are based on the principle of stress relaxation that occurs during cutting or drilling operations. However, characterisation of residual stresses to high confidence levels is notoriously difficult owing to the innate scatter in welding residual stress [11]. Undertaking residual stress measurements using multiple experimental techniques is crucial for robust validation of analytical or finite element models [12].

The substantial amount of data accumulated in recent years can be utilised for the application of data-driven models to predict the residual stresses in weldments; thereby finding potential applications in structural integrity assessment of power plant components. Machine learning techniques such as artificial neural networks (ANNs) and adaptive neuro-fuzzy inference systems (ANFIS) have been increasingly used as alternative prognostic methods for modelling complex problems associated with

engineering systems. Recently, ANNs have been applied to predict welding-induced residual stresses [13, 14] where the prediction was expressed as a distribution plot providing realistic uncertainty bounds. Ahmadzadeh *et al.* [15] presented ANNs for predicting residual stress distributions obtained from finite element data in gas-metal-arc weldments using a Levenberg-Marquardt training algorithm. The application of hybrid models based on support vector regression and neuro-evolutionary computing have also been proposed [16, 17] using datasets accumulated from finite element simulation. Na *et al.* developed a fuzzy neural network model for prediction of residual stresses in dissimilar metal welds using data from parametric finite element analysis [18]. More recently, Koo *et al.* [19] estimated the residual stresses in dissimilar metal welds in nuclear power plants using cascaded support vector regression. Alamaniotis *et al.* [20] studied the application of probabilistic kernel machines for predictive monitoring of welding residual stress in circumferentially welded pipes. The outcomes of these studies for predicting the residual stress state of weldments have been promising. However, there have been inadequate studies comparing the performance of different data-driven techniques for predicting residual stress distribution of welded components.

ANN and ANFIS models have been increasingly used for prediction and optimisation purposes using improved algorithms [21-24]. In this work, we present a novel application of ANN and ANFIS methods to predict residual stresses induced by welding for application in structural integrity assessment. The performance of ANN and ANFIS models can be effectively compared as the convergence criteria for training algorithms used in both neural networks and neuro-fuzzy systems is based on the minimisation of the error function over the given weight space. In supervised training, the error function is defined as the sum of square of the difference between

the desired and predicted output vectors. The problem of mapping inputs to outputs by operating gradient descent to minimise the error can be reduced to a common optimization problem.

In this study, we present: (1) ANN and ANFIS models to predict through-thickness residual stress profiles using experimental data, described in section 2.2 and 2.3 respectively; (2) Section 3.1 presents performance comparison of the proposed techniques based on statistical indicators such as root mean square (RMSE), absolute fraction of variance  $R^2$  and mean absolute percentage error (MAPE); (3) the generalisation ability of methods on test and training datasets (see section 3.1), and residual plots expressed as a function of individual input parameters (see section 3.2); and, (4) case studies demonstrating the efficacy of the ANN and ANFIS methods are discussed in section 3.3.

## 2 Material and methods

### 2.1 Database

Residual stress measurements in austenitic stainless steel girth welds collated over the last two decades were used to develop ANN and ANFIS models. These measurements were undertaken by diverse measurement techniques as part of UK nuclear power industry research programmes. The primary objective was to contribute to the knowledge gap in measured residual stress profiles, and to validate finite element simulations for assessing the structural integrity of engineering components. Neutron diffraction, the only non-destructive technique employed in this work, can achieve penetration depth of several centimetres and spatial resolution of the order of 1 mm in linear dimension. The contour method (CM) and deep hole drilling (DHD) methods were the preferred destructive techniques for measuring the through-wall

distribution of the residual stresses in welded mock-ups. Detailed information about the experimental measurements can be found in [25].

A schematic diagram defining the stress components and geometry of a pipe girth weld is shown in Fig. 1. The measurement database covers a wide range of welding heat input  $Q$  (kJ/mm), wall thickness ( $t$ ) and mean radius-to-wall-thickness ratio ( $R/t$ ), which are considered to be the key input parameters controlling the residual stress distribution in circumferentially welded pipes [26]. Details of the welded samples and input parameters used to simulate the axial and hoop residual stress profiles are described in Table 1. The forecasting models were trained and tested using randomly selected samples. A total of 278 and 338 samples were obtained in the axial and hoop stress direction respectively, of which 80% of the data were used for training and the remainder for testing purposes.

## **2.2 Artificial neural network (ANN)**

ANNs are abstract computational models inspired by the functionality of a biological neuron [27]. ANNs consist of processing elements called neurons that operate in a parallel and interconnected manner through the synaptic connections between multiple layers. The amplitude of a synaptic connection between two nodes, referred to as ‘weight’ and ‘bias’ parameters, are optimised during training. A multi-layer perceptron (MLP) [28], consisting of at least one hidden layer, is capable of representing non-linear relationships between the input and the output. The non-linear functions are usually sigmoidal-shaped, such as a log-sigmoid transfer function, because of the relative ease of determining derivatives and for adapting an appropriate input-output mapping. In a fully connected MLP, the input variables are connected to the neurons of the hidden layer and the outputs from these nodes are propagated to the output layer. The net output  $y$  from the output layer is represented by equation (1),

$$y = \sum_{k=1}^H w_k \log \left[ \sum_{i=1}^z w_{ij} p_i + b^{(1)} \right] + b^{(2)} \quad (1)$$

where  $w_{ij}$  is the weight vector of the hidden layer,  $w_k$  the weight vector of the output layer,  $b^{(1)}$  the bias of the hidden layer,  $b^{(2)}$  the bias of the output layer,  $z$  the number of input variables, and  $H$  is the number of hidden neurons.

Convergence to the optimal solution is based on the minimisation of the error function over the given weight space. The error function  $E(x, w)$  is defined as the sum of squares of the desired ( $d_k$ ) and predicted ( $p_k$ ) output vectors,

$$E(x, w) = \frac{1}{2} \sum_{k=1}^N \{d_k - p_k\}^2 \quad (2)$$

where  $x$  is the input vector,  $w$  the weight vector, and  $N$  the total number of data points.

Importantly, the search for the global optimum minimum of the error surface can be a tedious process and may well end with becoming trapped in local minima. Error back-propagation [29] is the most commonly used algorithm for training in pattern recognition problems. The algorithm is governed by the application of a chain rule in an iterative manner until the influence of each weight parameter is determined based on the error function of the form:

$$\frac{\partial E}{\partial w_{ij}} = \frac{\partial E}{\partial y_i} \frac{\partial y_i}{\partial net_i} \frac{\partial net_i}{\partial w_{ij}} \quad (3)$$

where  $w_{ij}$  is the weight matrix from neuron  $j$  to neuron  $i$ ,  $y_i$  the output, and  $net_i$  is the weighted sum of inputs of neurons  $i$ . Consequently, a gradient descent is operated with the objective of minimising the error function expressed as:

$$w_{ij}(t+1) = w_{ij}(t) - \varepsilon \frac{\partial E}{\partial w_{ij}}(t) \quad (4)$$

However, the use of the error back-propagation method can often lead to slow convergence owing to the increased dependence on the learning rate ( $\varepsilon$ ). A small learning rate would imply higher computational time and a trade-off approach is required to give the optimal learning rate in order to obtain the best global minima.

The use of resilient propagation (RPROP) [30] and Levenberg-Marquardt (LM) algorithms [31] are the possible alternatives to the conventional back-propagation algorithm, as they can arguably overcome the inherent drawbacks associated with the gradient descent techniques. The RPROP algorithm [30] is claimed to be an easy to implement scheme owing to its robustness against the choice of network parameters such as delta initial ( $\Delta_0$ ) and a reduced number of learning steps required to reach convergence. The sign of the derivative is a deciding factor of the direction of weight update and the individual weight values  $\Delta_{ij}$  are updated based on the learning rules expressed as follows:

$$\Delta w_{ij}(t) = \begin{cases} -\Delta_{ij(t)}, & \text{if } \frac{\partial E^{(t)}}{\partial w_{ij}} > 0 \\ +\Delta_{ij(t)}, & \text{if } \frac{\partial E^{(t)}}{\partial w_{ij}} < 0 \\ 0, & \text{else} \end{cases} \quad (5)$$

$$w(t+1) = w(t) + \Delta w_{ij}(t) \quad (6)$$

$$\Delta_{ij(t)} = \begin{cases} \eta^+ \Delta_{ij(t-1)}, & \text{if } \frac{\partial E}{\partial w_{ij}}^{(t-1)} \times \frac{\partial E}{\partial w_{ij}}^{(t)} > 0 \\ \eta^- \Delta_{ij(t-1)}, & \text{if } \frac{\partial E}{\partial w_{ij}}^{(t-1)} \times \frac{\partial E}{\partial w_{ij}}^{(t)} < 0 \\ \Delta_{ij(t-1)}, & \text{else} \end{cases} \quad (7)$$

where  $0 < \eta^- < 1 < \eta^+$

The LM algorithm combines the advantages of the steepest descent method, and the Gauss-Newton algorithm introduces an approximation of the Hessian matrix ( $H$ ) to be an invertible matrix of the form:

$$H \approx J^T J + \mu I \quad (8)$$

where  $\mu$  is defined as the combination coefficient,  $J$  is the Jacobian matrix of the error function with respect to the weights, and  $I$  is the identity matrix.

The update rule follows the Gauss-Newton algorithm for values of combination coefficient approaching zero. The weight update rule of the LM algorithm for a relatively large value of  $\mu$  can be expressed as a function of Jacobian and error vector ( $e$ ):

$$w(t+1) = w(t) - (J_t^T J_t + \mu I)^{-1} J_t e_t \quad (9)$$

### **2.3 Adaptive neuro-fuzzy inference systems (ANFIS)**

A neuro-fuzzy system [32, 33] is a combination of fuzzy logic and neural networks where the input-output relationship is constructed by the fuzzy inference system (FIS) and membership functions are tuned using an adaptive neural network. The learning capability of ANN is exploited to design the fuzzy IF-THEN rules and to adapt the semantic network parameters. The learning regime can be either performed using a backpropagation method or hybrid method (combination of least squares and backpropagation). The conceptual diagram of an ANFIS consists of five functional

components: fuzzifier, database, rulebase, inference engine, and defuzzifier (see Fig.

2). The fuzzifier transforms the numeric input parameters into linguistic fuzzy sets.

The database stores the values of the membership functions. The rulebase facilitates the definition of premises and consequences as fuzzy sets that represent all possible relationships between the input parameters and output. A fuzzy inference system implements a non-linear mapping of the input-output datasets formulated by the IF-THEN rules. The fuzzy inference engine takes into account all the rules in the fuzzy rule base and learns to transform a set of inputs to a given output through the use of inference operators such as minimisation (*min*) and product (*prod*). Subsequently, the defuzzifier is employed to translate the linguistic fuzzy sets back to the crisp form or a non-fuzzy real number.

The layer-by-layer operation of a fuzzy inference system assuming two input parameters  $x$  and  $y$ , with  $z$  as the output parameter, is demonstrated in Fig. 3. For a first-order Sugeno fuzzy model [30], the rule base consisting of two IF-THEN rules can be expressed as,

$$\text{Rule 1: If } x \text{ is } A_1 \text{ and } y \text{ is } B_1, \text{ then } f_1 = p_1x + q_1y + r_1 \quad (10)$$

$$\text{Rule 2: If } x \text{ is } A_2 \text{ and } y \text{ is } B_2, \text{ then } f_2 = p_2x + q_2y + r_2 \quad (11)$$

where  $p_i$ ,  $q_i$  and  $r_i$  (for  $i = 1$  or  $2$ ) are the linear parameters, and  $A_1$ ,  $B_1$ ,  $A_2$  and  $B_2$  are the non-linear parameters. The ANFIS structure is made of five layers: fuzzification layer, inference layer, normalisation layer, defuzzification layer and the output layer [30].

*Layer 1 (Input layer):* The fuzzification layer defines the membership function that is used to incorporate fuzziness in the fuzzy sets. The membership grade ( $O$ ) can be expressed using the membership function of the form:

$$O_{1,i} = \mu_{A_i}(x), \text{ for } i = 1, 2 \quad \text{or} \quad (12)$$

$$O_{I,i} = \mu_{Bj}(y), \text{ for } j = 1, 2 \quad (13)$$

where  $x$  and  $y$  is the input to node  $I$ , and  $A_i$  and  $B_j$  is the corresponding linguistic label associated with the node. Membership function of the form  $\mu_{Ai}(x)$  or  $\mu_{Bj}(y)$  is typically denoted using a Gaussian or bell-shaped function having a magnitude of unit interval  $[0, 1]$ . These functions inherently hold the advantage of representing non-linear relationships owing to the flexibility and continuous nature of their derivatives. The bell-shaped function is defined as a set of three fitting parameters  $\{a, b, c\}$ ,

$$\mu_{Ai}(x) = \frac{1}{1 + \left[ ((x - c)/a)^2 \right]^b} \quad (14)$$

The parameters in this layer are referred to as the premise part of the fuzzy IF-THEN rules, as they control the shape of the membership function.

*Layer 2 (Rule node):* The AND operator (labelled as “Π”) is then applied to the corresponding degrees obtained from the input layer, resulting in the generation of firing strengths as the subsequent output denoted as  $(O_{2,k})$ . The most commonly used fuzzy AND operators are the *min* or *prod*. The output is expressed as:

$$O_{2,k} = w_k = \mu_{Ai}(x) \times \mu_{Bj}(y), \text{ for } k = 1 \text{ to } 4 \quad (15)$$

*Layer 3 (Normalized layer labelled “N”):* In this layer, the firing strength ( $w_k$ ) is normalised by following a simple transformation: *i.e.*, the ratio of each of the  $i$ th's rule firing strength to the sum of all rules firing strength is calculated using the equation:

$$O_{3,k} = w_i^n = \frac{w_i}{w_1 + w_2 + w_3 + \dots + w_k} \quad (16)$$

*Layer 4 (Consequent node):* The contribution of the  $i$ th's rule towards the final output parameter is determined in this layer. This is represented as the consequent parameter set  $\{p_i, q_i, r_i\}$  of the Sugeno fuzzy model:

$$O_{4,k} = w_i f_i = w_i (p_i x + q_i y + r_i) \quad (17)$$

*Layer 5 (Output layer):* The overall output  $\Sigma$  is computed by summing all the incoming signals using the equation,

$$O_{5,k} = \sum w_i f_i = \frac{\sum_i^4 w_i f_i}{\sum_i^4 w_i} \quad (18)$$

The premise parameters of the ANFIS membership function are tuned by employing the gradient descent method (used in backpropagation algorithm) or the hybrid algorithm based on the combination of gradient descent and least-square methods. In the backpropagation algorithm, the error function is calculated as the sum of squared difference between the network output and the desired output. The error function with respect to each node is then computed and subsequently propagated backwards to adapt the network parameters in order to satisfy the global minima criteria [34]. However, the learning process can stop with the error function becoming trapped in a local minimum and this can affect the network performance. In the latter approach, the non-linear parameters, also described as ‘premise’ parameters ( $\{a, b, c\}$ ), are fixed in the forward pass. The output can therefore be expressed as a linear combination of consequent parameters optimised using the least-squares method. The error function is then determined using the sum of squares error from the actual and desired output parameters. In the backward pass, the consequent parameters ( $\{p_i, q_i, r_i\}$ ) remain unchanged and the premise parameters are optimised using the gradient descent method. The hybrid method is known to converge faster than conventional backpropagation as it reduces the dimensionality of the search space.

## 2.4 Implementation

The performance and efficacy of the developed ANN and ANFIS models are subjected to robust comparison by a wide range of methods. The gradient descent method is used to evaluate the ANN parameters and ANFIS premise parameters but are governed by the local minimum stopping criteria. The models employed in this study are summarized as follows:

*ANN-1*: Artificial neural network trained using resilient backpropagation algorithm

*ANN-2*: Artificial neural network trained using Levenberg-Marquardt algorithm

*FNN-1*: Fuzzy neural network trained using backpropagation algorithm

*FNN-2*: Fuzzy neural network trained using hybrid method (combination of backpropagation and least squares method)

All input parameters and output were normalised in the range  $-1$  to  $1$  by simple linear transformation. All methods were undertaken with four inputs (welding heat input, radius/thickness, wall thickness and through-wall position) and one output (residual stress) using the MATLAB neural network and fuzzy logic toolbox [35].

Table 2 summarizes the network parameters of the *ANN-1* and *ANN-2* methods. For the sake of comparison, the number of epochs was set to 1000 for all models. The number of neurons in the hidden layer essentially controls the complexity of the neural network model and should be optimised to prevent overfitting. An iterative procedure was followed by evaluating the test and training error as a function of the number of hidden neurons (see Fig. 4). The ANN architecture used in this study is shown in Fig. 5. The neural network weights are initialised with small random values to prevent premature saturation of the sigmoid functions [36]. Conversely, this would result in having different predictions each time the network is run. As a consequence, an ensemble of 100 networks with the same architecture were formed and the best

network was chosen based on minimum test error criteria. The network parameters used for training the fuzzy neural network methods *FNN-1* and *FNN-2* are summarised in Table 3. Fig. 6 provides a schematic illustration of the ANFIS architecture used in this study. Generalised bell-type (*Gbellmf*) was the chosen input membership function based on minimum root mean square error using the test data and the most consistent of all. For instance, several membership functions were attempted such as Gaussian (*gaussmf*), triangular shaped (*trimf*), trapezoidal shaped (*trapmf*), Gaussian combination (*gauss2mf*), sigmoidal shaped (*sigmf*), and  $\Pi$  shaped (*pimf*). The total number of rules used in *FNN-1* and *FNN-2* methods were 256 and 81 respectively, as training with four membership functions could not be performed in *FNN-2* owing to computational limitations. The statistics of the measured and predicted residual stress data using the training and test datasets obtained from different models are summarised in Table 4. Fig. 7 present the pseudocode of the proposed methods using ANN and ANFIS. For validation of the predictions, the holdout method was primarily used by randomly dividing into training and test datasets. Note, 80% of the data was used for training and remaining for testing purposes. The leave-one-out cross validation technique was also employed in the case studies to compare the residual stress profiles predicted by ANN and ANFIS.

### 3 Results and Discussions

#### 3.1 Benchmark criteria for comparing performance of ANN and ANFIS methods

The model performance is evaluated by both numerical and visual methods. Visual methods can provide an intuitive representation of the model performance whereas statistical indicators can provide robust means of model comparison from a scientific

point of view [37]. The performance of the models was assessed using root-mean-square error (*RMSE*), absolute fraction of variation ( $R^2$ ), and mean absolute percentage error (*MAPE*) as described in equations (19), (20) and (21),

$$RMSE = \sqrt{\frac{1}{N} \sum_i (a_i - p_i)^2} \quad (19)$$

$$R^2 = 1 - \left( \frac{\sum_i (a_i - p_i)^2}{\sum_i p_i^2} \right) \quad (20)$$

$$MAPE = \frac{1}{N} \sum_i \left| \frac{(a_i - p_i)}{p_i} \right| \times 100 \quad (21)$$

where  $a_i$  is the actual residual stress,  $p_i$  the predicted residual stress, and  $N$  the sample size.

Statistical performance indicators can give a quantitative estimate of how well a predictive model has performed based on the actual and predicted data. The performance indices for predicting residual stresses in the axial and hoop directions are given in Table 5. The statistical values *RMSE*,  $R^2$ , and *MAPE* for training and testing data from the ANN methods for axial and hoop stresses clearly revealed the superior predictive performance of the *ANN-2* model over *ANN-1*. Likewise, the statistical indicators from the ANFIS methods demonstrate superior predictive performance of *FNN-2* model in comparison with *FNN-1*.

In the axial residual stress prediction, the lowest *RMSE* error in training is observed with *FNN-2* followed by *ANN-2*, then *FNN-1* and *ANN-1*. This trend is also repeated with the RMSE error of the testing data. The  $R^2$  parameter follows a recurrent pattern with the training and testing data sets. However, the only exception was with the *MAPE* statistical indicator where the lowest error in training has been achieved by *ANN-2* closely followed by *FNN-2*. Overall, the performance of different

models for predicting axial residual stresses solely based on statistical indicators can be summarized as  $FNN-2 > ANN-2 > FNN-1 > ANN-1$ . With the hoop residual stresses,  $ANN-2$  outperforms  $FNN-2$  in the case of  $RMSE$  test ( $RMSE_{ANN-2} = 0.0939$ ,  $RMSE_{FNN-2} = 0.1444$ ),  $R^2$  test ( $R^2_{ANN-2} = 0.9677$ ,  $R^2_{FNN-2} = 0.9258$ ) and  $MAPE$  training error ( $MAPE_{ANN-2} = 19.9089$ ,  $MAPE_{FNN-2} = 33.0865$ ). Hence it is difficult to select the best method for the prediction of hoop stresses. Therefore, the performance of different techniques based on statistical indicators can be ranked as  $FNN-2$  or  $ANN-2 > FNN-1 > ANN-1$ .

Scatter plots of the predicted versus observed data are an efficient way to visualise the data and evaluate the model's performance. It is good practice to present the predicted versus measured plots using independent training and test datasets as the former can provide a measure of the fitting uncertainty whereas the latter represents the generalisation ability of the network to perform in unseen datasets. Fig. 8 shows the comparison of predicted and measured results for the axial residual stresses using the ANN methods. Fig. 8(a) and (b) show the predicted (in the Y-axis) and observed (in the X-axis) residual stresses using  $ANN-1$  and  $ANN-2$  models with the training data; and 8(c) and (d) show the comparison with the test data. Fig. 9 shows the predicted versus observed plots using the neuro-fuzzy models following the same sequence. Interestingly, the dataset comprising axial residual stress profiles is much noisier than the hoop stresses as evident from the scatter plots.

To summarize, the  $ANN-2$  model (trained using Levenberg-Marquadt algorithm) performs superior to the  $ANN-1$  model (trained using resilient back-propagation). In the case of neuro fuzzy models,  $FNN-2$  (trained using hybrid method) outperforms  $FNN-1$  (trained using back-propagation) as demonstrated in Fig. 9. Consistent trends are observed with the predicted and measured plots of hoop residual stresses as

evident in Figs. 10 and 11. Hence it was a relatively simple task to select the best individual model among the ANN and FNN methods. However, the selection of the single best model remains indecisive between the *ANN-2* and *FNN-2* models from the observations here. The following sections discuss further studies undertaken to compare the performance of these methods.

### **3.2 Residual plots as a function of input variables**

Residual plots are used to improve the understanding of the regression models by identifying the presence of any systematic error. For this purpose, the residuals (difference between predicted and measured values) are plotted as a function of the individual input parameters. For instance, it can be inferred that the input variables used in the predictive model are insufficient to capture crucial information in the data if the residual plot reveals the presence of non-random patterns. It can potentially represent scenarios where there is a missing variable, sometimes in a higher order form, or missing interaction of the variables used in the model. In contrast, the model can be improved if there is evidence of systematic error in the residual plots. Fig. 12 shows the comparison of the residual plots for predicting axial stresses as a function of the through-wall position, radius/thickness ratio, wall-thickness and welding heat input for training and test data. Residual plots were evenly distributed with no obvious pattern, suggesting the absence of any systematic error. Furthermore, the plots are mostly symmetrically distributed with the mean centred around zero (along the Y axis) throughout the range of fitted variables following a Gaussian distribution. The pattern observed in residual plots of hoop stresses were matching with the residual plots of axial stresses (see Fig. 13). As envisaged, both *ANN-2* and *FNN-2* methods are able to capture the non-linear patterns in the residual stress data. Moreover, this study confirms that the input parameters used in these models were able to specify the

required mapping without the need for including additional variables. However, it was not distinguishable from the residual plots as to which model is superior.

### ***3.3 Case studies demonstrating the efficacy of different methods***

The model predictions are compared with experimental measurements to evaluate the efficacy of the *ANN-2* and *FNN-2* models. The leave-one-out cross validation technique was used in case studies shown in Figs. 14 and 15. This approach was attempted for four cases each using axial and hoop residual stress data. In Fig. 14, the residual stress profiles along the axial direction are compared with experimental measurements undertaken using neutron diffraction, contour method and deep hole drilling in welded mock-ups. Fig. 14(a) shows the predicted and measured residual stress profile in sample MU4-3 ( $R/t = 4.5$ ,  $t = 25\text{mm}$ ,  $Q = 1.5 \text{ kJ/mm}$ ). There is a significant amount of scatter between the residual stress measurements using neutron diffraction and the contour method. This is not unusual considering the innate scatter found in weld residual stresses [11]. Both *ANN-2* and *FNN-2* model predictions are in reasonable agreement with the measurements, however the *ANN-2* profile is non-conservative in the through-wall position range ( $x/t$ ) from 0.3 to 0.7 with regard to both neutron and contour measurements. The *FNN-2* profile is slightly better in comparison with the *ANN-2* profile. This is repeatedly seen in the axial stress profile of sample S5New ( $R/t = 2.8$ ,  $t = 65\text{mm}$ ,  $Q = 0.8 \text{ kJ/mm}$ ) in Fig. 14(d) where the *ANN-2* profile underestimates the measured stresses using deep hole drilling from through wall position  $x/t$  between 0.6 - 0.9. The stress profiles predicted by *ANN-2* and *FNN-2* models are in excellent agreement in mock-ups ES ( $R/t = 2.1$ ,  $t = 35\text{mm}$ ,  $Q = 1.6 \text{ kJ/mm}$ ) and SP37 ( $R/t = 5.3$ ,  $t = 37\text{mm}$ ,  $Q = 1.68 \text{ kJ/mm}$ ) as shown in Figs. 13 (b) and (c) respectively. The hoop residual stress profiles from different models and experimental measurements are given in Fig. 15. Good agreement is seen with most

of the measurements through the thickness and the predicted residual stresses in sample MU4-3 (refer Fig. 15 (a)). Some discrepancy is observed only with the neutron measurements near the inside and outside surfaces of the pipe. In Fig. 15 (b) the contour method measurements near the surfaces are in good agreement with the ANN-2 and FNN-2 predictions. Despite this, there is slight under-prediction by ANN close to the outside surface. The through-wall residual stress profiles are in excellent agreement with the deep hole drilling measurements in mock-ups SP37 and S5New (see Fig. 15 (c) and (d)).

In fracture assessment procedures [1, 2] the three dimensional (3-D) distribution of the residual stresses in a welded joint is usually simplified by assuming a representative 1-D profile of the stress tensor through the thickness. The stress intensity factor of the postulated crack is calculated from the representative 1-D profile that is assumed to be acting normal to the crack path. As a consequence, the residual stress profile assumed in these calculations can have a critical influence on the outcome of fracture assessments. In fact, this would determine whether defects are repaired, components replaced or whether a rigorous inspection regime need to be implemented to monitor further degradation. It has been demonstrated that the ANN-based prediction expressed as a distribution plot can be effectively used to provide a reliable prediction interval of the residual stress distribution in weldments [13, 14].

However, in this study, the performance of two independent machine learning techniques based on ANN and ANFIS are evaluated based on several benchmarks.

Overall, the performance of the ANN and ANFIS models are acceptable and could serve as surrogate models for predicting residual stresses in welds. The application of these data-based models compared to the finite element approach is relatively simple and does not require comprehensive information for generating accurate results. The

superiority of the ANFIS compared to ANN model is realised in the case studies shown in Fig. 14 and Fig. 15 where the *ANN-2* model tends to underestimate the magnitude of residual stresses significantly: an example is shown in Fig. 14 (d) where under-prediction of tensile stresses in excess of 150 MPa is reported. This is possibly due to the better local interpolation capabilities of ANFIS compared to the ANN that tries to develop a generalised relationship. Moreover, the performance of *FNN-2* is found to be slightly better in application to axial data which exhibits more noise, with the respective error values in the test data:  $RMSE = 0.1264$ ,  $R^2 = 0.9102$ , and  $MAPE = 22.9442$  compared to *ANN-2* error values:  $RMSE = 0.1486$ ,  $R^2 = 0.8719$ , and  $MAPE = 48.0591$ . Nevertheless, residual stress data associated with welding inherently exhibits a high level of noise and this is considered as a drawback if the model is to be used in safety-critical assessment of welded components. Additionally, the ANFIS method was more time consuming though has better ease of implementation without the need for any post processing. By contrast, the best network of the ANN has to be selected from the ensemble of networks based on the test error making the total processing time higher than that of the ANFIS method. To conclude, taking into account all the factors discussed above, the overall performance of ANFIS model *FNN-2* is slightly better than the *ANN-2* model. ANFIS trained using hybrid algorithm has reportedly given more realistic predictions than the ANN model trained Levenberg-Marquadt in all the case studies presented. The ANFIS method can be further developed as a reliable prediction model for structural integrity assessments of defective plant thereby reducing the susceptibility to be overly conservative by a large margin, avoiding unnecessary and costly repair or inspection. However, the application of the model requires the construction of a comprehensive database covering greater neutron diffraction, contour method and surface measurements. Furthermore, as a caveat,

appropriate fracture sensitivity studies should be undertaken and suitable margins of safety has to be included prior to the application of the proposed model.

## Conclusions

1. Artificial Neural Network (ANN) and Adaptive Neuro-Fuzzy Inference System (ANFIS) models were developed that can predict through-thickness residual stress profiles in stainless steel pipe girth welds. The performance of different models was evaluated, using statistical indicators and scatter plots obtained from training and test datasets as the benchmark.
2. ANN trained using Levenberg-Marquadt, and ANFIS based on a hybrid algorithm, were far superior to ANN model trained by resilient-backpropagation and ANFIS using backpropagation method. However, it was not possible to determine a single best method from the statistical performance indicators and scatter plots.
3. Residual plots were found to be evenly distributed displaying non-random patterns suggesting there is no missing variable, or missing interaction of the variables used in the model. ANN trained using Levenberg-Marquadt method and ANFIS using hybrid algorithm are able to capture the non-linear patterns in the residual stress data confirming the ability to specify the required mapping without the need for additional variables.
4. The ANFIS model based on a hybrid algorithm performed better than the ANN model trained using Levenberg-Marquadt, as the latter tends to underestimate the tensile residual stresses by a large margin as high as 150 MPa. This is possibly due to the better local interpolation capabilities of

ANFIS compared to the ANN that tries to develop a generalised relationship.

Moreover, the performance of ANFIS based on a hybrid method is regarded as better in axial data prediction which exhibits more noise, with the respective error values in the test data:  $RMSE = 0.1264$ ,  $R^2 = 0.9102$ , and  $MAPE = 22.9442$  compared to the ANN error values:  $RMSE = 0.1486$ ,  $R^2 = 0.8719$ , and  $MAPE = 48.0591$ .

5. ANFIS trained using a hybrid algorithm has reportedly given more realistic predictions than the ANN model trained Levenberg-Marquadt. The ANFIS method can be further developed as a reliable prediction model for structural integrity assessments of defective plant thereby reducing the susceptibility to be overly conservative by a large margin, avoiding unnecessary and costly repair or inspection. However, for the application of the model in fracture assessments, the construction of a comprehensive database covering greater neutron diffraction, contour method and surface measurements is essential.

### Acknowledgements

Jino Mathew and Michael Fitzpatrick are grateful for funding from the Lloyd's Register Foundation (LRF), a charitable foundation helping to protect life and property by supporting engineering-related education, public engagement and the application of research. John Bouchard, Richard Moat and Sanjoram Paddea are gratefully acknowledged for their contribution in acquiring experimental measurements. EDF Energy and AMEC Process and Power are acknowledged for funding the experimental studies.

## References

- [1] R6 Revision 4 Assessment of the integrity of structures containing defects., Gloucester, 2009.
- [2] API 579-1/ASME FFS-1, Fitness-for-Service, Second, 2007.
- [3] Lindgren, L.-E. Computational welding mechanics. Thermomechanical and microstructural simulations, Woodhead Publishing Ltd., Cambridge, 2007.
- [4] S.K. Bate, P.J. Bouchard, The Validation of Weld Residual Stresses for Use in Structural Integrity Assessment, *Appl. Mech. Mater.* 70 (2011) 297–302.
- [5] M.C. Smith, P.J. Bouchard, M. Turski, L. Edwards, R.J. Dennis, Accurate prediction of residual stress in stainless steel welds, *Comp. Mater. Sci.* 54 (2012) 312–328.  
doi:10.1016/j.commatsci.2011.10.024
- [6] M.C. Smith, A.C. Smith, Advances in weld residual stress prediction: A review of the NeT TG4 simulation round robin part 1, thermal analyses, *Int. J. Press. Vessel. Pip.* (2017). doi:10.1016/j.ijpvp.2017.11.003.
- [7] M.C. Smith, A.C. Smith, Advances in weld residual stress prediction: A review of the NeT TG4 simulation round robin part 2, mechanical analyses, *Int. J. Press. Vessel. Pip.* Accepted Manuscript, (2017). doi:10.1016/j.neubiorev.2017.04.006.
- [8] Hutchings, M.T., Withers P.J, Holden, T.M., Lorentzen, T. Introduction to characterization of residual stress by neutron diffraction, Taylor & Francis, 2005.
- [9] M.B. Prime, Cross-sectional mapping of residual stresses by measuring the surface contour after a cut, *J. Eng. Mater. Technol.* 123 (2001) 162–168.
- [10] D.J. Smith, P.J., Bouchard, P.J., D. George, Measurement and prediction of residual stresses in thick-section steel welds, *J. Strain Anal.* 35 (2000) 287–305.

- [11] P.J. Bouchard, Code characterisation of weld residual stress levels and the problem of innate scatter, *Int. J. Press. Vessel. Pip.* 85 (2008) 152–165.  
doi:10.1016/j.ijpvp.2007.10.013.
- [12] M.C. Smith, A.C. Smith, R. Wimpory, C. Ohms, A review of the NeT Task Group 1 residual stress measurement and analysis round robin on a single weld bead-on-plate specimen, *Int. J. Press. Vessel. Pip.* 120–121 (2014) 93–140.  
doi:10.1016/j.ijpvp.2014.05.002.
- [13] J. Mathew, R.J. Moat, S. Paddea, M.E. Fitzpatrick, P.J. Bouchard, Prediction of residual stresses in girth welded pipes using an artificial neural network approach, *Int. J. Press. Vessel. Pip.* 150 (2017) 89–95.
- [14] J. Mathew, R.J. Moat, S. Paddea, J. Francis, M.E. Fitzpatrick, P.J. Bouchard, Through-Thickness Residual Stress Profiles in Austenitic Stainless Steel Welds: A Combined Experimental and Prediction Study. *Metall. Mater. Trans. A* 48 (2017) 6178–6191.
- [15] M. Ahmadzadeh, A. Hoseini Fard, B. Saranjam, H.R. Salimi, Prediction of residual stresses in gas arc welding by back propagation neural network, *NDT E Int.* 52 (2012) 136–143. doi:10.1016/j.ndteint.2012.07.009.
- [16] J. Edwin Raja Dhas, S. Kumanan, Evolutionary fuzzy SVR modeling of weld residual stress, *Appl. Soft Comput. J.* 42 (2016) 423–430. doi:10.1016/j.asoc.2016.01.050.
- [17] J. Edwin Raja Dhas, S. Kumanan, Neuro evolutionary model for weld residual stress prediction, *Appl. Soft Comput. J.* 14 (2014) 461–468. doi:10.1016/j.asoc.2013.08.019.
- [18] M.G. Na, J.W. Kim, D.H. Lim, Y.-J. Kang, Residual stress prediction of dissimilar metals welding at NPPs using support vector regression, *Nucl. Eng. Des.* 238 (2008) 1503–1510. doi:10.1016/j.nucengdes.2007.12.003.

- [19] Y. D. Koo, K. H. Yoo, M.G. Na, Estimation of Residual Stress in Welding of Dissimilar Metals at Nuclear Power Plants Using Cascaded Support Vector Regression, *Nucl. Eng. Technol.* 49 (2017) 817-824.
- [20] M. Alamaniotis, J. Mathew, A. Chroneos, M.E. Fitzpatrick, L.H. Tsoukalas, Probabilistic kernel machines for predictive monitoring of weld residual stress in energy systems, *Eng. Appl. Artif. Intell.* 71 (2018) 138–154.  
doi:10.1016/j.engappai.2018.02.009.
- [21] İ. Toktaş, A. T. Özdemir, Artificial neural networks solution to display residual hoop stress field encircling a split-sleeve cold expanded aircraft fastener hole, *Expert Syst. Appl.* 38 (2011) 553–563. doi:10.1016/j.eswa.2010.06.102.
- [22] M. Prauzek, P. Krömer, J. Rodway, P. Musilek, Differential evolution of fuzzy controller for environmentally-powered wireless sensors, *Appl. Soft Comput. J.* 48 (2016) 193–206. doi:10.1016/j.asoc.2016.06.040.
- [23] R.E. Precup, M.C. Sabau, E.M. Petriu, Nature-inspired optimal tuning of input membership functions of Takagi-Sugeno-Kang fuzzy models for Anti-lock Braking Systems, *Appl. Soft Comput. J.* 27 (2015) 575–589. doi:10.1016/j.asoc.2014.07.004.
- [24] S. Chaki, B. Shanmugarajan, S. Ghosal, G. Padmanabham, Application of integrated soft computing techniques for optimisation of hybrid CO<sub>2</sub> laser–MIG welding process, *Appl. Soft Comput. J.* 30 (2015) 365–374. doi:10.1016/j.asoc.2015.01.045.
- [25] P.J. Bouchard, Validated residual stress profiles for fracture assessments of stainless steel pipe girth welds, *Int. J. Press. Vessel. Pip.* 84 (2007) 195–222.  
doi:10.1016/j.ijpvp.2006.10.006.

- [26] S. Song, P. Dong, X. Pei, A full-field residual stress estimation scheme for fitness-for-service assessment of pipe girth welds: Part I – Identification of key parameters, *Int. J. Press. Vessel. Pip.* 126–127 (2015) 58–70. doi:10.1016/j.ijpv.2015.01.002.
- [27] Bishop, C.M. *Neural networks for Statistical Pattern Recognition*. Oxford University Press, United Kingdom, 1994.
- [28] K. Hornik, M. Stinchcombe, H. White, *Neural Networks*. 2 (1989) 359–366.
- [29] D. E. Rumelhart, G. E. Hinton, Learning representations by back-propagating errors, *Nature*. 323 (1986) 533–536.
- [30] M. Riedmiller, H. Braun. A direct adaptive method for faster backpropagation learning: The RPROP algorithm. In *Proceedings of the IEEE International Conference on Neural Networks*, IEEE Press (1993) 586–591.
- [31] H. Yu, B.M. Wilamowski, Levenberg-Marquardt training, *Ind. Electron. Handbook*, Vol. 5 – *Intell. Syst.* (2011) 12, 1-18.
- [32] J.S.R. Jang, C.T. Sun, E. Mizutani, *Neuro-Fuzzy Soft Comput*, Prentice Hall, New Jersey, 1997.
- [33] J.S.R. Jang, ANFIS – Adaptive-network-based fuzzy inference system, *IEEE Trans. Syst. Man. Cybern.* 23 (1993) 665–685.
- [34] T. Takagi, M. Sugeno, Fuzzy identification of systems and its applications to modeling and control, *IEEE Trans. Syst. Man. Cybern.* 15 (1985) 116–132.
- [35] MATLAB: Neural Network and Fuzzy Logic Toolbox, The MathWorks Inc., Natick, Massachusetts, USA, 2015.

- [36] L.H. Tsoukalas, R.E. Uhrig, Fuzzy and neural approaches in engineering, John Wiley & Sons, Inc. New York, 1996.
- [37] M.K. Kolehmainen, Data exploration with self-organizing maps in environmental informatics and bioinformatics, 2004, Ph.D. thesis.

## Tables and Figures

Table 1. Experimental residual stress measurements considered for training ANN and ANFIS methods.

<i>Sample</i>	<i>Measurement technique</i>	<i>Axial</i>	<i>hoop</i>	<i>R/t</i>	<i>t / mm</i>	<i>Q / kJ mm<sup>-1</sup></i>	<i>Welding process</i>
Weld C	BRSL	✓	✓	25	15.9	2.2	SAW
SP19	ND	✓	✓	10.5	19.6	1.12	MMA
SP37	DHD	✓	✓	5.3	37	1.68	MMA
S5VOR	DHD	✓	✓	2.8	65	1.92	MMA
S5Old	DHD	✓	✓	2.8	65	1.12	MMA
S5New	DHD	✓	✓	2.8	65	0.8	MMA
S5NG	DHD	✓	✓	3	62	1.32	TIG
RR	DHD	✓	✓	1.8	110	1.8	SAW
ES	CM	✓	✓	2.1	35	1.6	MMA
MU4-1	ND, CM	✓	✓	4.5	25	0.8	TIG
MU4-3	ND, CM	✓	✓	4.5	25	1.5	TIG
HI-1	CM	✗	✓	10	12.7	0.7	TIG
HI-2	CM	✗	✓	10	12.7	1	TIG
HI-3	CM	✗	✓	10	12.7	1.2	TIG

ND – Neutron diffraction, CM – Contour method, DHD – Deep hole drilling,  
 BRSL – Block removal splitting and layering, SAW – Submerged arc welding, MMA –  
 Manual metal arc, TIG – Tungsten inert gas.

Table 2. Summary of network parameters used in *ANN-1* and *ANN-2* models

<b><i>Network parameters</i></b>	<b><i>Description</i></b>
<b><i>ANN-1</i></b>	
Maximum Epochs	1000
Minimum Gradient	$1 \times 10^{-5}$
Initial Delta ( $\Delta_o$ )	0.07
Delta Increase	1.2
Delta Decrease	0.5
Maximum Delta	50
<b><i>ANN-2</i></b>	
Maximum Epochs	1000
Minimum Gradient	$1 \times 10^{-7}$
Mu ( $\mu$ )	0.001
Mu Decrease Ratio	0.1
Mu Increase Ratio	10
Maximum Mu	10000000000

Table 3. Summary of network structure and optimised parameters used in *FNN-1* and *FNN-2* models

<i>Network parameters</i>	<i>Description</i>
Structure	Anfis
Inference type	Sugeno
Inputs/Outputs	[4 1]
Optimisation method	Back-propagation and hybrid
Number of Input MFs	[4 4 4 4], [3 3 3 3]
Number of Rules	256, 81
And Method	<i>prod</i>
Or Method	<i>max</i>
Implication Method	<i>prod</i>
Aggregation Method	<i>max</i>
De-fuzzification Method	<i>wtaver</i>
Input MF Type	<i>gbellmf</i>
Output MF Type	<i>linear</i>

Table 4. Statistics of the measured and predicted residual stress data using the training and test datasets obtained from different models

<i>Parameters</i>	<i>Training data (measured)</i>	<i>Test data (measured)</i>	<i>Training data (ANN-1)</i>	<i>Test data (ANN-1)</i>	<i>Training data (ANN-2)</i>	<i>Test data (ANN-2)</i>	<i>Training data (FNN-1)</i>	<i>Test data (FNN-1)</i>	<i>Training data (FNN-2)</i>	<i>Test data (FNN-2)</i>
<i>axial</i>										
<i>min</i>	-349.944	-249.039	-204.481	-201.9642	-247.7680	-234.3655	-270.5293	-221.6483	-303.5297	-214.8795
<i>max</i>	293.0957	249.5774	219.8427	216.1368	285.4549	237.9690	257.2752	230.4091	289.4758	225.5226
<i>mean</i>	-6.33678	-17.9077	-6.79863	-24.2108	-8.2278	-24.5074	-6.2044	-23.6103	-6.3368	-17.8269
<i>standard deviation</i>	130.9542	130.893	115.2594	114.66	126.0583	122.1449	122.7308	121.1497	127.8505	125.2831
<i>hoop</i>										
<i>min</i>	-455.015	-396.4473	-370.9826	-358.1118	-455.2891	-400.4690	-416.1978	-416.1049	-460.632	-389.85
<i>max</i>	553.3863	418.4731	418.6781	398.1341	441.9873	404.6196	418.0949	406.3432	436.8114	452.8854
<i>mean</i>	101.7146	92.57275	101.6249	96.93421	100.4464	93.11098	101.4538	99.64614	101.7147	94.49121
<i>standard deviation</i>	217.6353	216.7005	208.2263	208.0546	219.0329	215.8434	211.6192	209.4099	216.2381	219.1166

Table 5. Comparison of statistical performance indicators for predicting axial and hoop residual stresses by different methods used in this study.

<i>Performance indicator</i>	<i>ANN-1</i>	<i>ANN-2</i>	<i>FNN-1</i>	<i>FNN-2</i>
<i>axial</i>				
<i>RMSE</i> training	0.1894	0.1162	0.1337	0.0883
<i>RMSE</i> test	0.1655	0.1486	0.1501	0.1264
<i>R</i> <sup>2</sup> training	0.7579	0.9238	0.8935	0.9571
<i>R</i> <sup>2</sup> test	0.8204	0.8719	0.8669	0.9102
<i>MAPE</i> training	99.1335	41.0222	64.2955	46.0874
<i>MAPE</i> test	51.1335	48.0591	51.9166	22.9442
<i>hoop</i>				
<i>RMSE</i> training	0.1264	0.0581	0.0990	0.0529
<i>RMSE</i> test	0.1389	0.0939	0.1102	0.1444
<i>R</i> <sup>2</sup> training	0.9397	0.9882	0.9640	0.9901
<i>R</i> <sup>2</sup> test	0.9258	0.9677	0.9543	0.9258
<i>MAPE</i> training	49.5157	19.9089	37.4735	33.0865
<i>MAPE</i> test	51.0772	26.7454	38.9118	23.7976

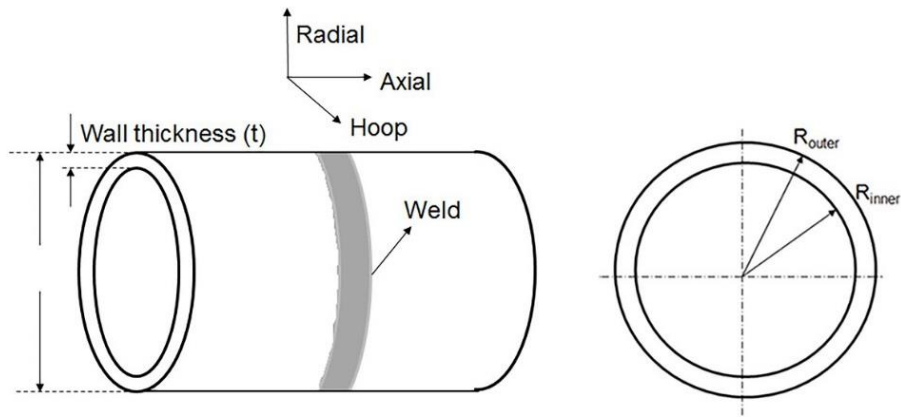


Fig. 1. Schematic illustration of a circumferential pipe-butt weld showing the residual stress components.

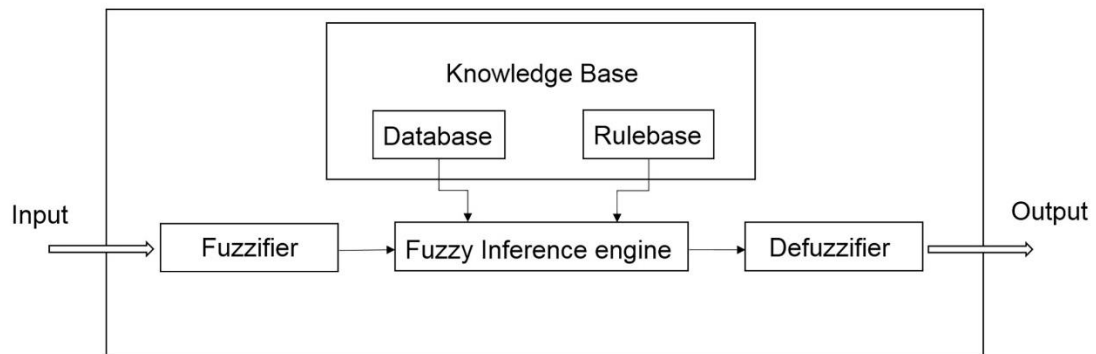


Fig. 2. Conceptual diagram of the fuzzy inference system

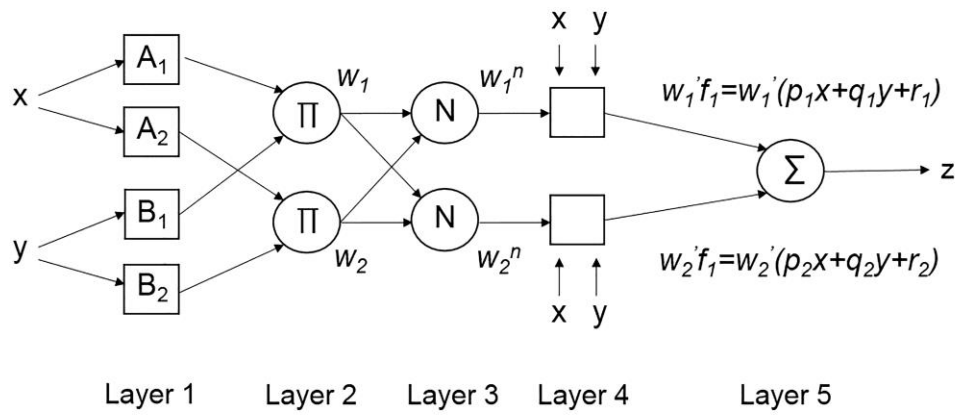


Fig. 3. Layer structure of a two-input Sugeno fuzzy ANFIS model

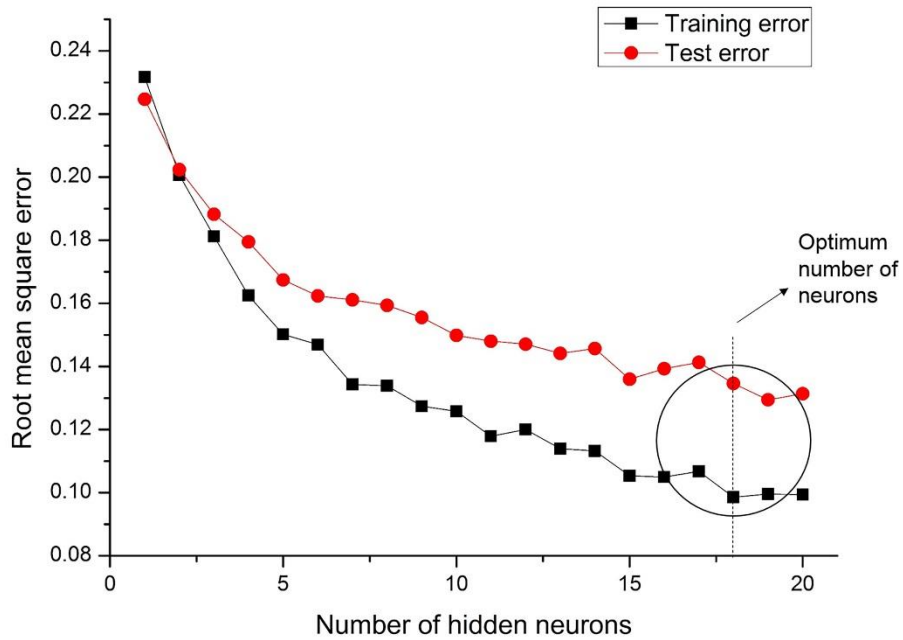


Fig. 4. Optimisation of the number of hidden neurons based on an iterative procedure comparing root-mean-square errors in training and testing scenarios.

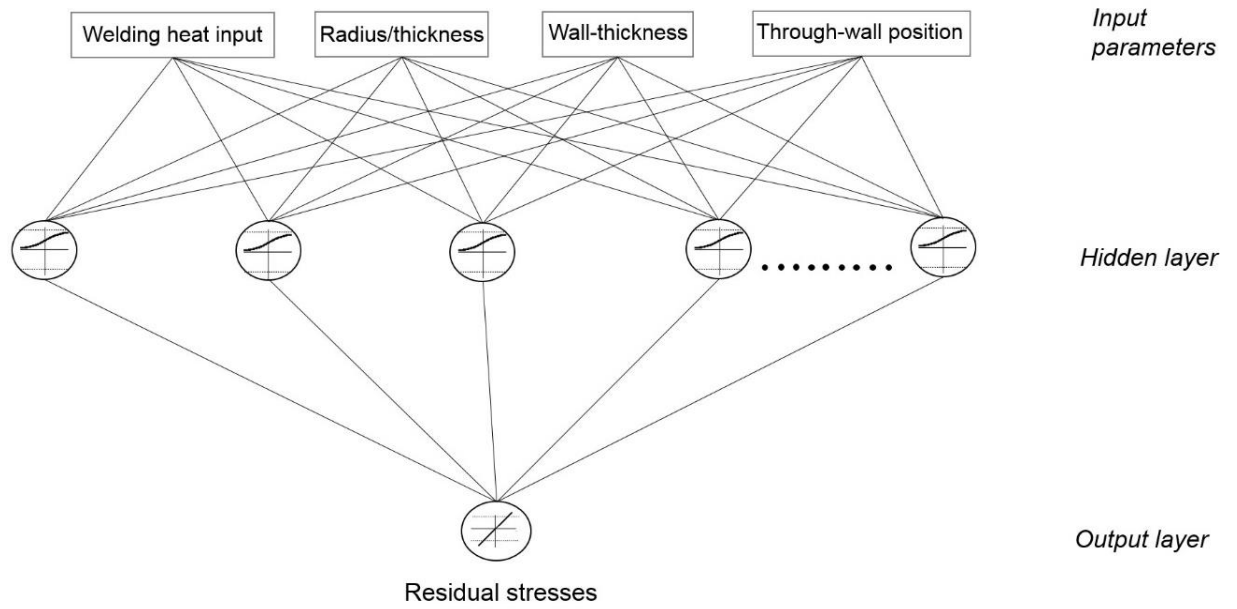


Fig. 5. Schematic representation of artificial neural network architecture representing the input parameters and output used in this study. Log-sigmoid activation function with 18 neurons was used in the hidden layer and linear function used in the output layer.

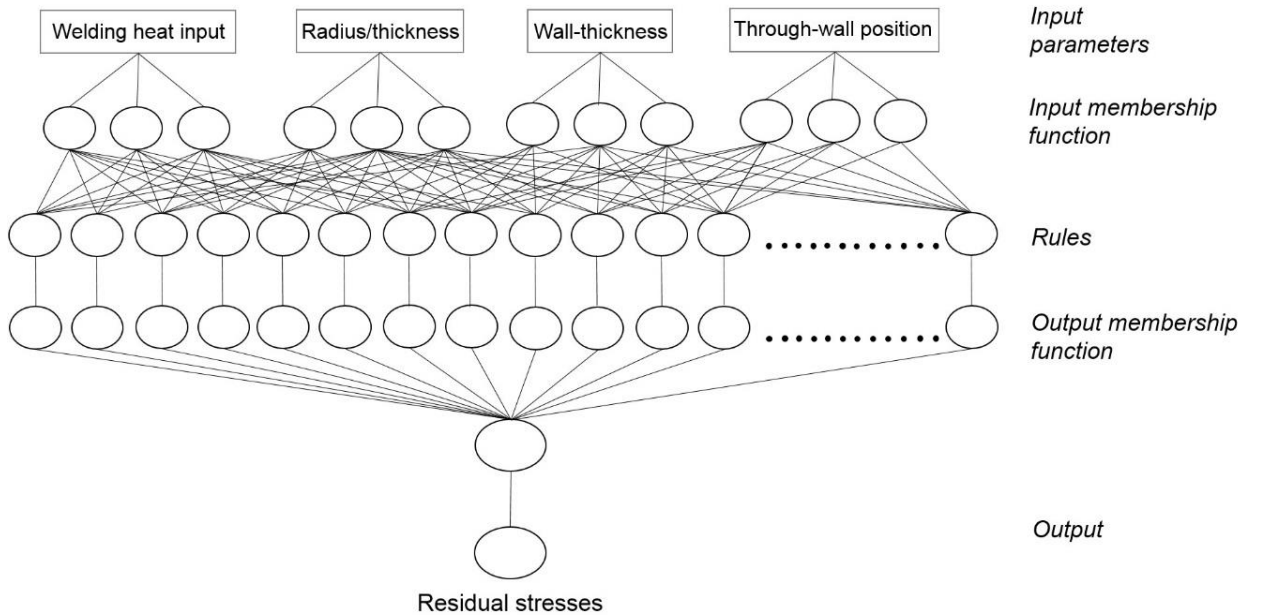


Fig. 6. Schematic representation of ANFIS architecture based on Sugeno-type fuzzy model representing the input parameters and output used in this study. *Gbellmf* function was used in the input layer and linear function used in the output layer. Total number of rules used in *FNN-1* and *FNN-2* methods were 256 and 81 respectively.

Input data: Training data set comprising welding heat input  $Q$  (kJ/mm), wall thickness ( $t$ ) and mean radius-to-wall-thickness ratio ( $R/t$ ). Through-thickness position ( $x/t$ )

Target variable: Residual stress parameter

#### ANN methods

BEGIN

1. Load trainingdata.mat
2. For( $n = 0$ ;  $n < 100$ ;  $n++$ )
  - {
  - 2.1 Init network
    - 2.1.1 Initialise weights, hidden layer and output activation function
    - 2.1.2 Assign maximum of training epochs
    - 2.1.3 Choose optimal number of neurons  $n$
  - 2.2 Train the neural network using 'trainlm' and 'trainrp' algorithm
    - 2.2.1 Optimise weights  $w_k$  and biases  $b^{(1)}, b^{(2)}$
    - 2.2.2 Stopping criteria reached? Train next network
  - }
- End
3. Choose best network based on the performance
4. Evaluate statistical performance indicators
 
$$Rms_{(test, training)} = \sqrt{\text{mean}((a[i] - p[i])^2)}$$

$$R^2_{(test, training)} = 1 - (\text{sum}((a[i] - p[i])^2) / \text{sum}((a[i])^2))$$

$$Error[i] = (a[i] - p[i])$$

$$MAPE_{(test, training)} = 100 * \text{mean}(\text{abs}(Error[i]/a[i]))$$
5. Generate predictions for hold-out or leave-one-out validation
6. Post process results

END

#### FNN methods

BEGIN

1. Load trainingdata.mat
2. Init network
  - 2.1 Init membership functions and membership number
  - 2.2 Init anfis type, and.method, or.method, defuzz.method, imp.method and agg.method
- 3 Define FIS
- 4 Assign maximum number of epochs
- 5 Train the fuzzy neural network using optmethod = 0,1 (0 = backpropagation, 1= hybrid algorithm)
  - 5.1 Create If-then rules
  - 5.2 Optimise step size
  - 5.3 Tune premise and consequent parameters
  - 5.3 Stopping criteria reached? proceed to step 6
- 6 Evaluate statistical performance indicators
 
$$Rms_{(test, training)} = \sqrt{\text{mean}((a[i] - p[i])^2)}$$

$$R^2_{(test, training)} = 1 - (\text{sum}((a[i] - p[i])^2) / \text{sum}((a[i])^2))$$

$$Error[i] = (a[i] - p[i])$$

$$MAPE_{(test, training)} = 100 * \text{mean}(\text{abs}(Error[i]/a[i]))$$
- 7 Generate predictions for hold-out or leave-one-out validation
- 8 Post process results

END

Fig. 7. Pseudocode of the proposed methods using ANN and ANFIS

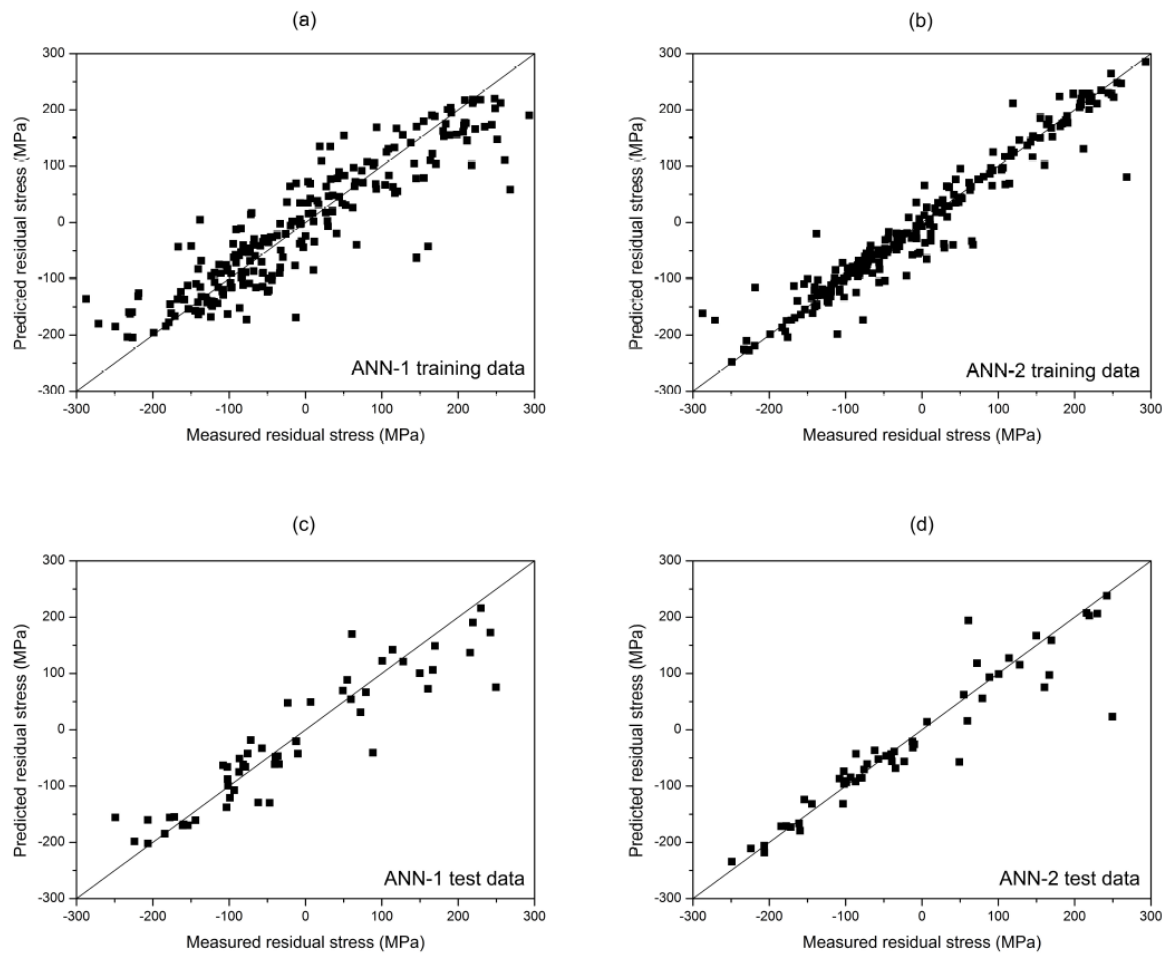


Fig. 8. Comparison of predicted and measured residual stress in axial direction for: (a) ANN-1 using training data; (b) ANN-2 using training data; (c) ANN-1 using test data; and (d) ANN-2 using test data.

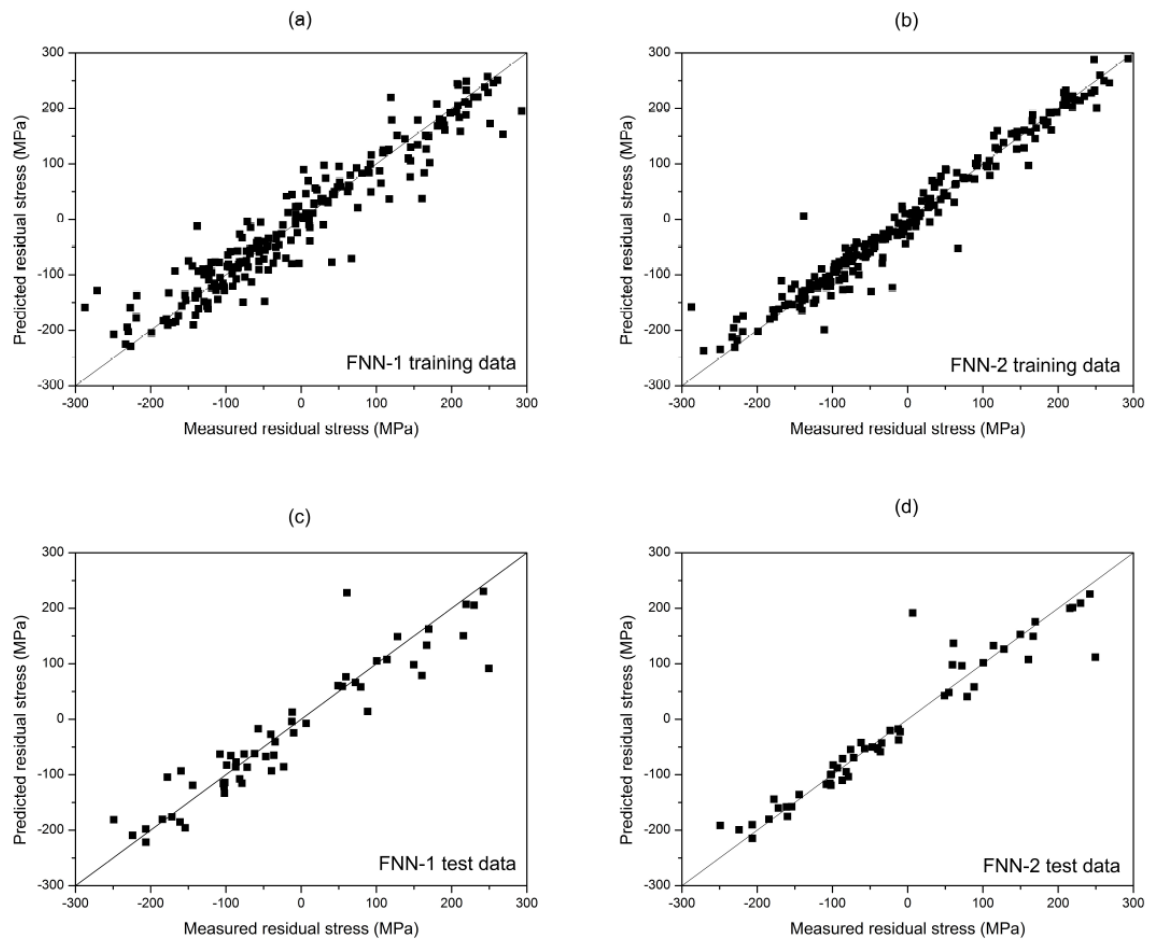


Fig. 9. Comparison of predicted and measured residual stress in axial direction for: (a) *FNN-1* using training data; (b) *FNN-2* using training data; (c) *FNN-1* using test data; and (d) *FNN-2* using test data.

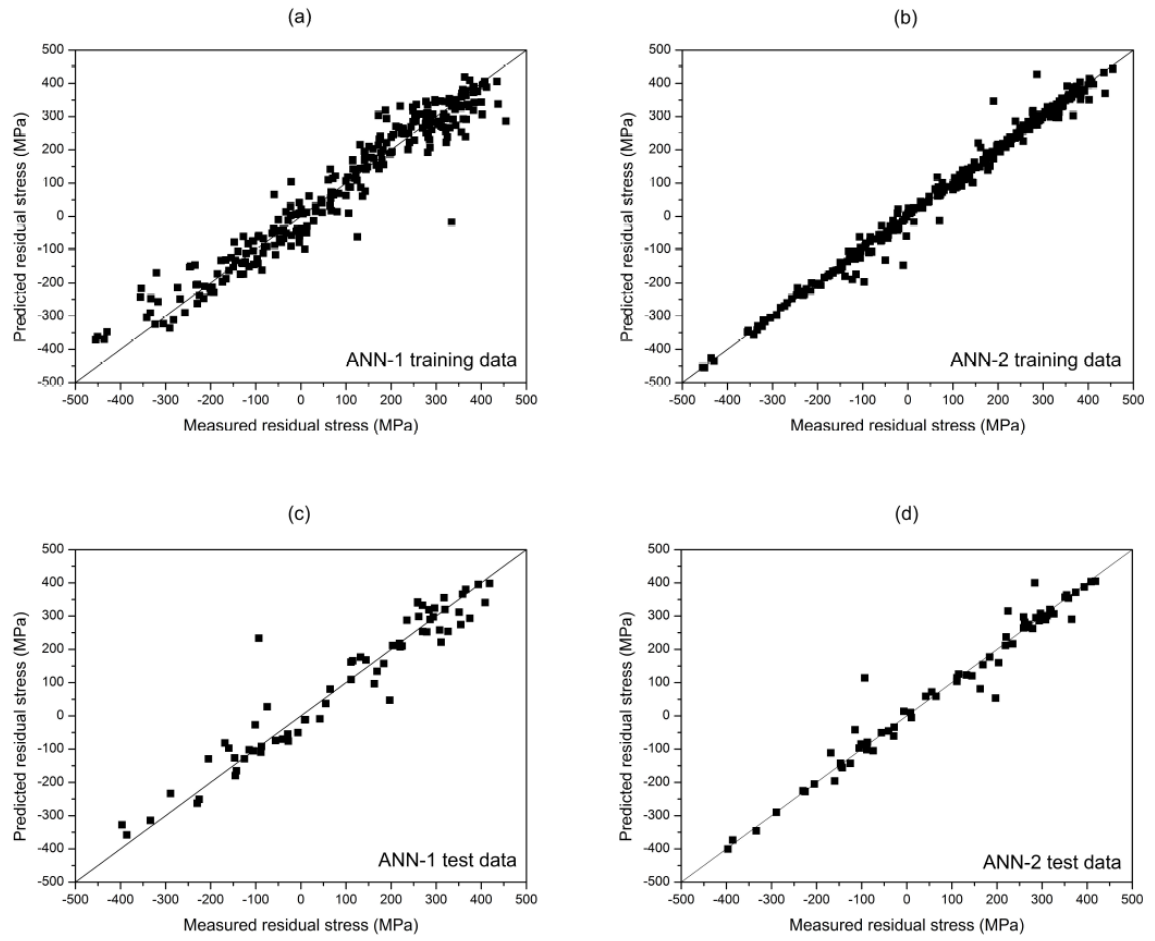


Fig. 10. Comparison of predicted and measured residual stress in hoop direction for:  
 (a) ANN-1 using training data; (b) ANN-2 using training data; (c) ANN-1 using test  
 data; and (d) ANN-2 using test data.

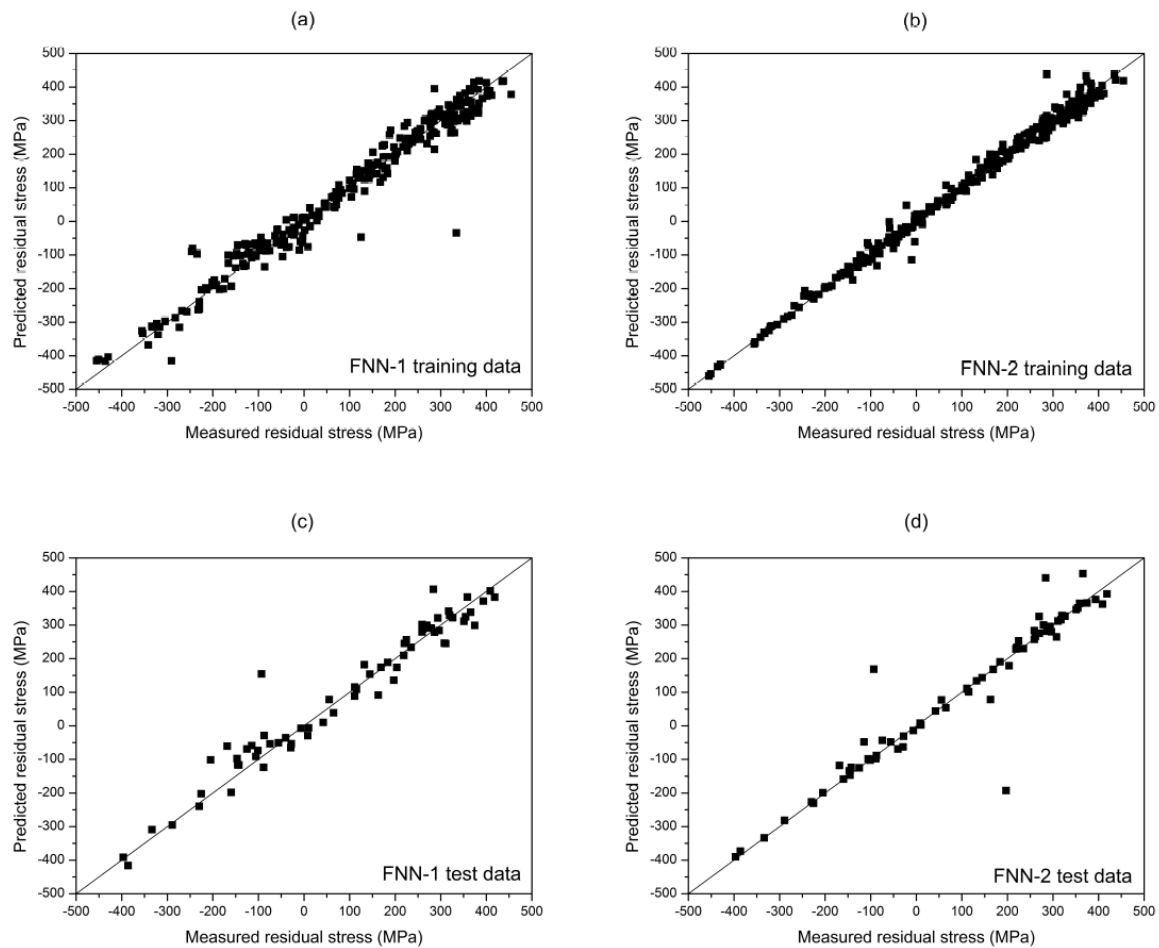


Fig. 11. Comparison of predicted and measured residual stress in hoop direction using: (a) *FNN-1* using training data; (b) *FNN-2* using training data; (c) *FNN-1* using test data; and (d) *FNN-2* using test data.

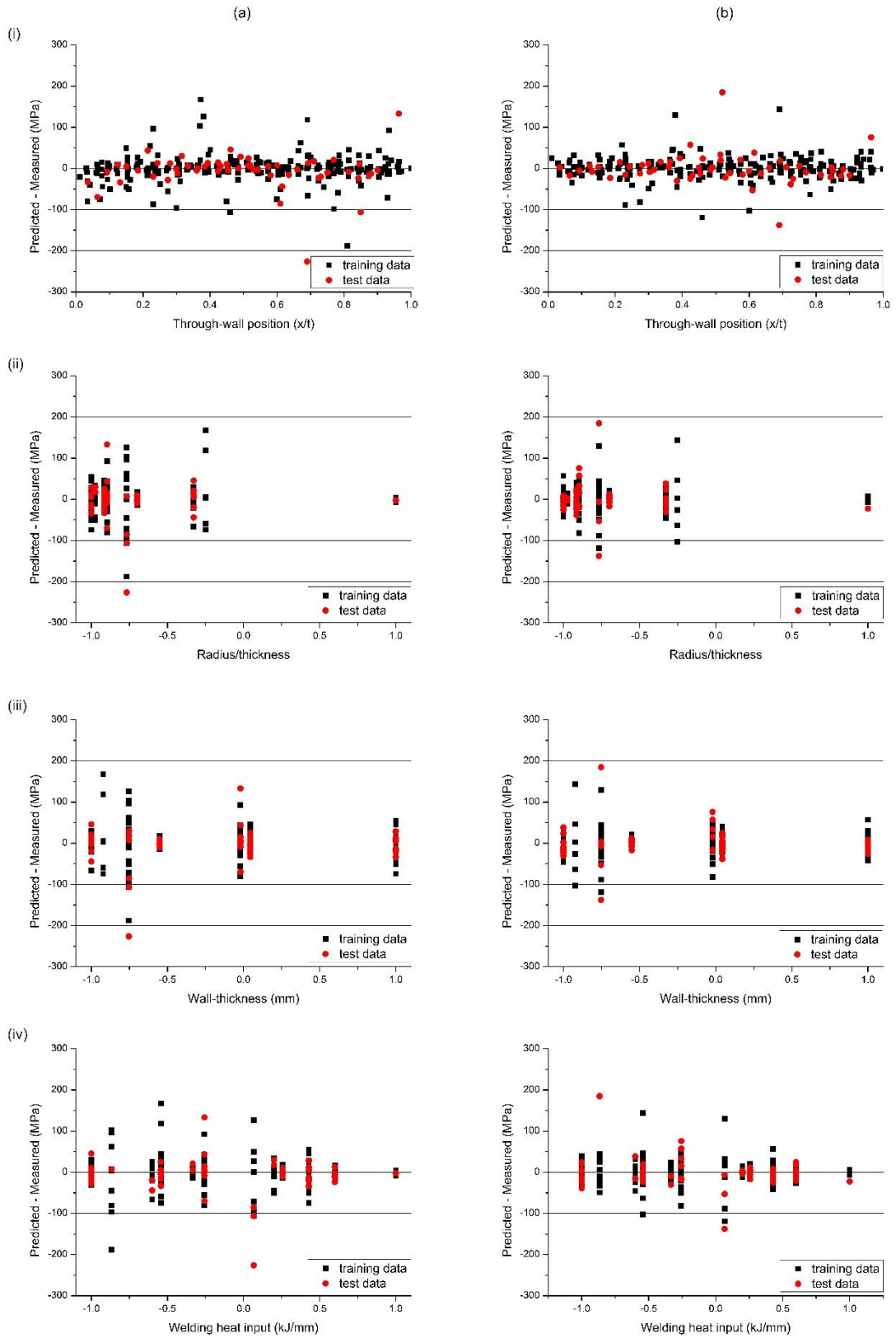


Fig. 12. Comparison of residual plots using (a) ANN-2 method and (b) FNN-2 method for predicted axial stresses as a function of input variables: (i) through-wall position; (ii) Radius/thickness; (iii) wall-thickness; (iv) welding heat input.

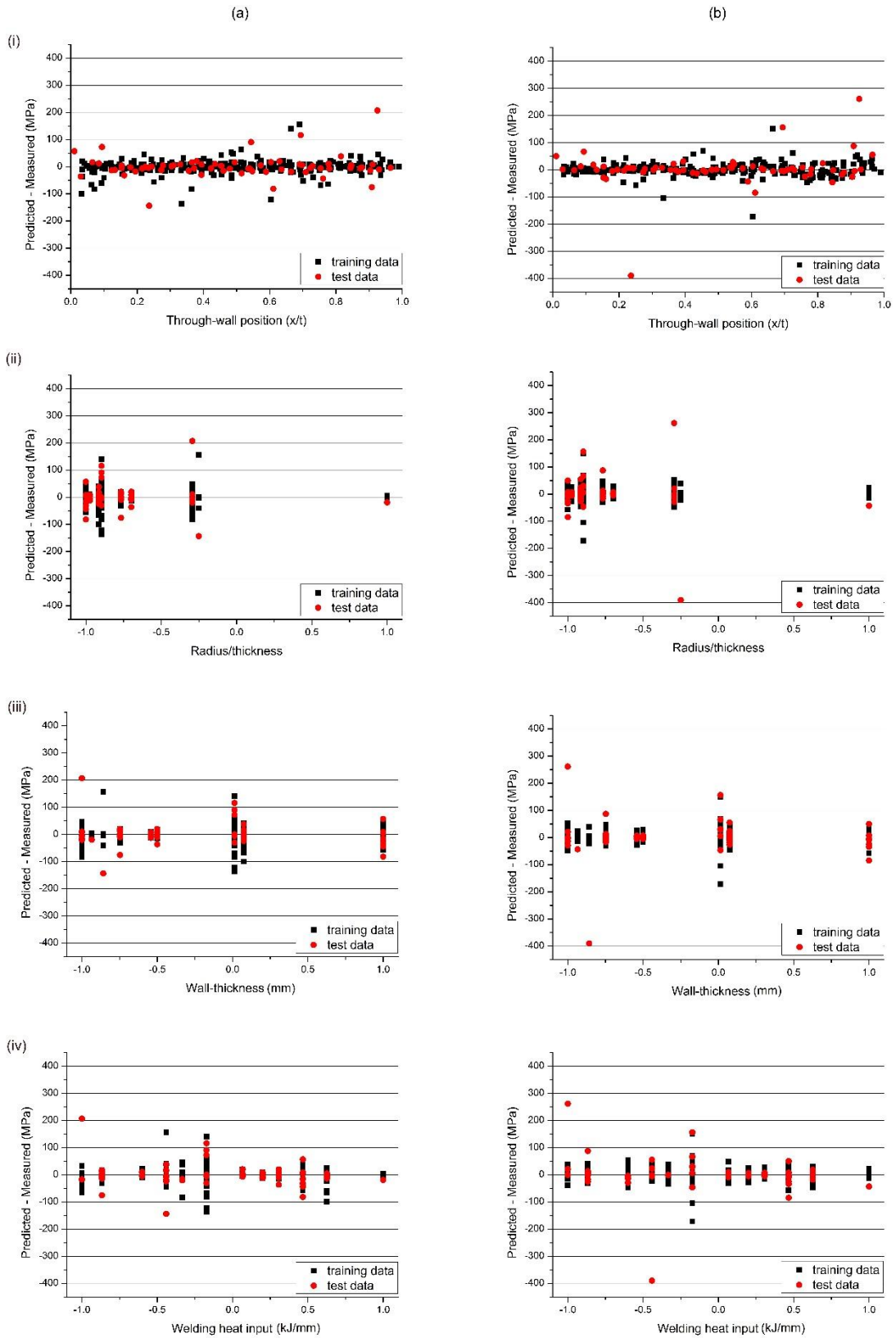


Fig. 13. Comparison of residual plots using (a) ANN-2 method and (b) FNN-2 method for predicted hoop stresses as a function of input variables: (i) through-wall position; (ii) Radius/thickness; (iii) wall-thickness; (iv) welding heat input.

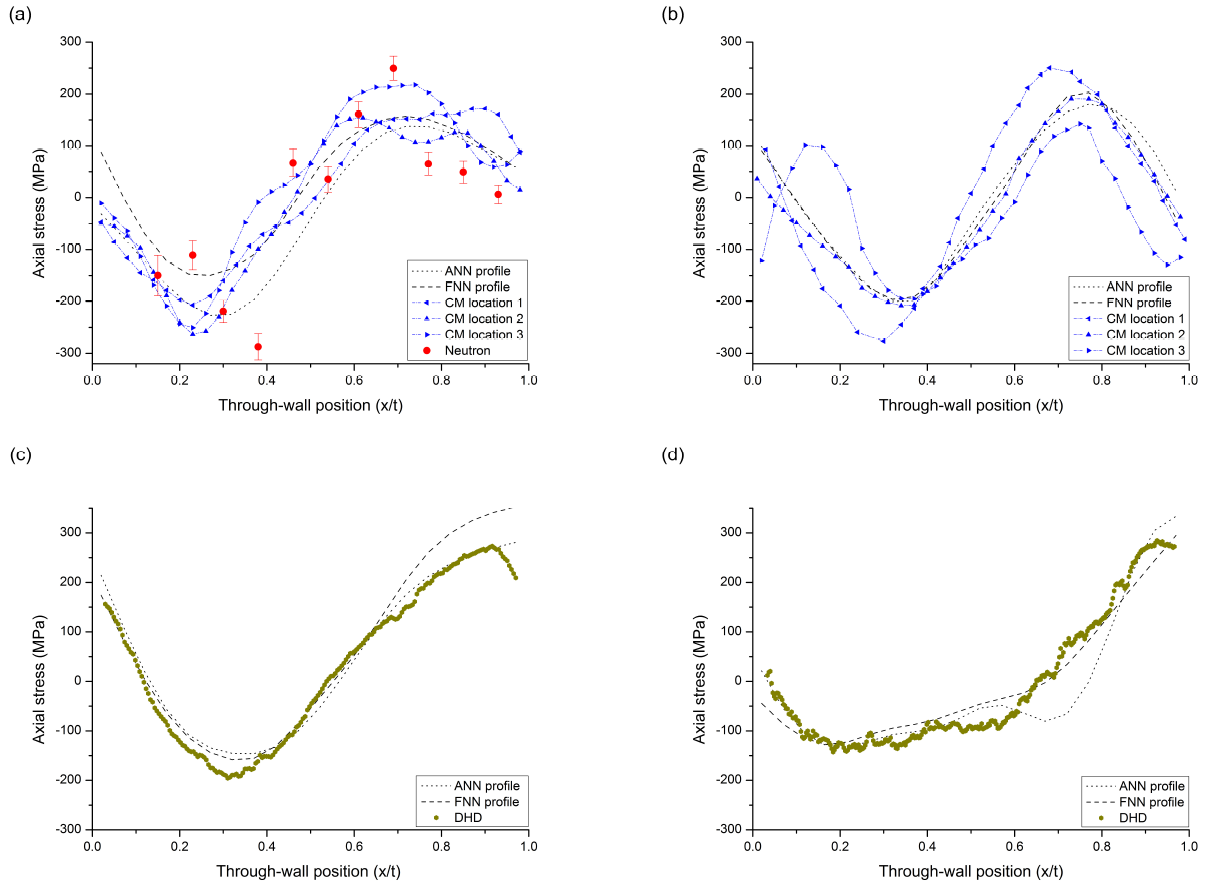


Fig. 14. Case studies showing the performance of ANN and FNN methods for the predicted axial residual stresses in welded mock-ups (a) MU4-3 (b) ES (c) SP37 and (d) S5New.

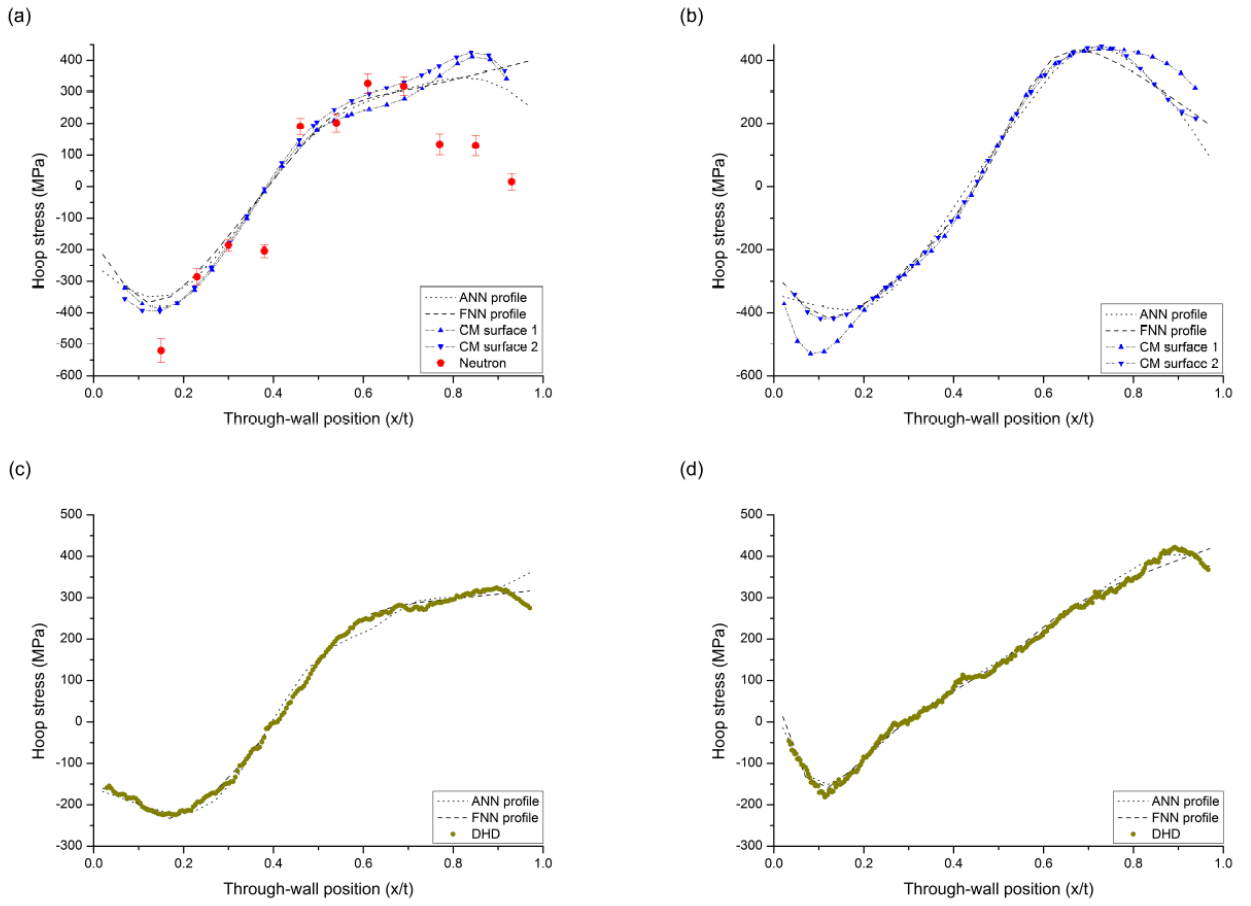


Fig. 15. Case studies showing the performance of ANN and FNN methods for the predicted hoop residual stresses in welded mock-ups (a) MU4-3 (b) ES (c) SP37 and (d) S5New.